

Charge-Density Wave in Ca-Intercalated Bilayer Graphene Induced by Commensurate Lattice Matching

Ryota Shimizu,¹ Katsuaki Sugawara,¹ Kohei Kanetani,² Katsuya Iwaya,¹ Takafumi Sato,² Takashi Takahashi,^{1,2} and Taro Hitosugi¹

¹*Advanced Institute for Materials Research (AIMR), Tohoku University, Sendai 980-8577, Japan*

²*Department of Physics, Tohoku University, Sendai 980-8578, Japan*

(Received 27 August 2014; published 7 April 2015)

We report the emergence of a charge-density wave (CDW) in Ca-intercalated bilayer graphene (C_6CaC_6), the thinnest limit of superconducting C_6Ca , observed by low-temperature, high-magnetic-field scanning tunneling microscopy or spectroscopy, and angle-resolved photoemission spectroscopy. While the possible superconductivity was not observed in epitaxially grown C_6CaC_6 on a SiC substrate, a CDW order different from that observed on the surface of bulk C_6Ca was observed. It is inferred that the CDW state is induced by the potential modulation due to the commensurate lattice matching between the C_6CaC_6 film and the SiC substrate.

DOI: [10.1103/PhysRevLett.114.146103](https://doi.org/10.1103/PhysRevLett.114.146103)

PACS numbers: 68.65.Pq, 71.45.Lr, 73.20.At, 74.70.Wz

The intercalation of metals into graphene sheets has attracted considerable attention since it drastically modifies the electronic structure and creates novel properties, absent in the host material [1–3]. One of the most intriguing phenomena in graphite intercalation compounds (GICs) is the emergence of superconductivity in the hybrid of otherwise nonsuperconducting graphite and metals. Just after the discovery of graphene [4], intensive efforts were made to fabricate superconducting graphene from both basic and application points of view. Ca-intercalated bilayer graphene (C_6CaC_6) is a promising candidate because Ca-intercalated GIC (C_6Ca) has the highest superconducting transition temperature of 11 K among the various metal-intercalated GICs [3]. A number of theoretical [5,6] and experimental [7] studies have reported that C_6CaC_6 should have an electronic structure similar to that of superconducting GICs, [8–10] indicating the possibility of superconductivity in C_6CaC_6 . On the other hand, it has been also suggested that the charge-density wave (CDW) may appear as a ground state to suppress the superconductivity in the metal intercalated bilayer graphene [11–13]. CDW is a periodic modulation of the electron density accompanied by the distortion of lattices, creating a variety of novel properties in low-dimensional materials. Since the coexistence or competition of superconductivity with CDW is one of the central issues in low-dimensional systems such as transition metal dichalcogenides, it is essential to elucidate the electronic structure in the ground state to address the controversy in metal-intercalated bilayer graphene.

In this Letter, we report the results of scanning tunneling microscopy or spectroscopy (STM/STS) and angle-resolved photoemission spectroscopy (ARPES) on epitaxially grown C_6CaC_6 to resolve the long-standing issue of the possibility of superconductivity in metal-intercalated bilayer graphene. We observed that the superconductivity

in C_6CaC_6 is hindered and that the CDW is induced by the potential modulation due to the commensurate lattice matching between the C_6CaC_6 film and the SiC substrate. This suggests that the superconducting state may compete with the CDW state induced by the Fermi-surface nesting of the π^* band.

Bilayer graphene was prepared by heating an *n*-type Si-rich 6H-SiC(0001) single crystal to 1550 °C with resistive heating under Ar gas at 0.1 MPa. The growth of bilayer graphene was confirmed by the number of π bands (two) observed in the ARPES measurement. C_6LiC_6 was fabricated by depositing lithium on the bilayer graphene at room temperature using a lithium dispenser (SAES Getters) [14]. For the fabrication of C_6CaC_6 , calcium was deposited on C_6LiC_6 with a Knudsen cell at a sample temperature of 140 °C under ultrahigh vacuum of 5×10^{-10} Torr, and it was subsequently heated above 145 °C to replace the Li atoms with Ca atoms [7]. After fabricating C_6CaC_6 , we transferred the sample to the STM or ARPES system without breaking the vacuum. The STM system was operated using a Unisoku USM-1300S at 5 and 78 K [15]. STM images were obtained in a constant current mode, and each dI/dV curve was obtained by numerical differentiation of the original I - V curves. All five samples showed the $5/2a_{C_6CaC_6}$ CDW modulation at 5 K. ARPES measurements were performed at Tohoku University, using a VG-Scienta SES2002 electron analyzer with a high-intensity helium discharge lamp and a toroidal grating monochromator. For the excitation of photoelectrons, we used the He II α resonance line ($h\nu = 40.814$ eV). The energy and angular resolutions were set at 16 meV and 0.2°, respectively. The sample was kept at 30 K during the ARPES measurements. The Fermi level of the samples was referenced to that of a gold film evaporated onto the sample holder.

Figures 1(a)–1(f) show the STM images taken at 5 K and the corresponding fast-Fourier transform (FFT) images for bilayer epitaxial graphene (BEG), C_6LiC_6 , and C_6CaC_6 . In the STM image of BEG, we clearly see the hexagonal lattice with a reciprocal lattice vector of G_{BEG} , together with the

$(6\sqrt{3} \times 6\sqrt{3})$ moiré pattern produced by the interference between the graphene sheet and the SiC substrate [16]. On intercalating Li into BEG, the $(6\sqrt{3} \times 6\sqrt{3})$ moiré pattern vanishes, while additional sharp $(\sqrt{3} \times \sqrt{3}) - R30^\circ$ spots ($G_{C_6LiC_6}$) appear in the k space [Fig. 1(e)] [7]. Furthermore,

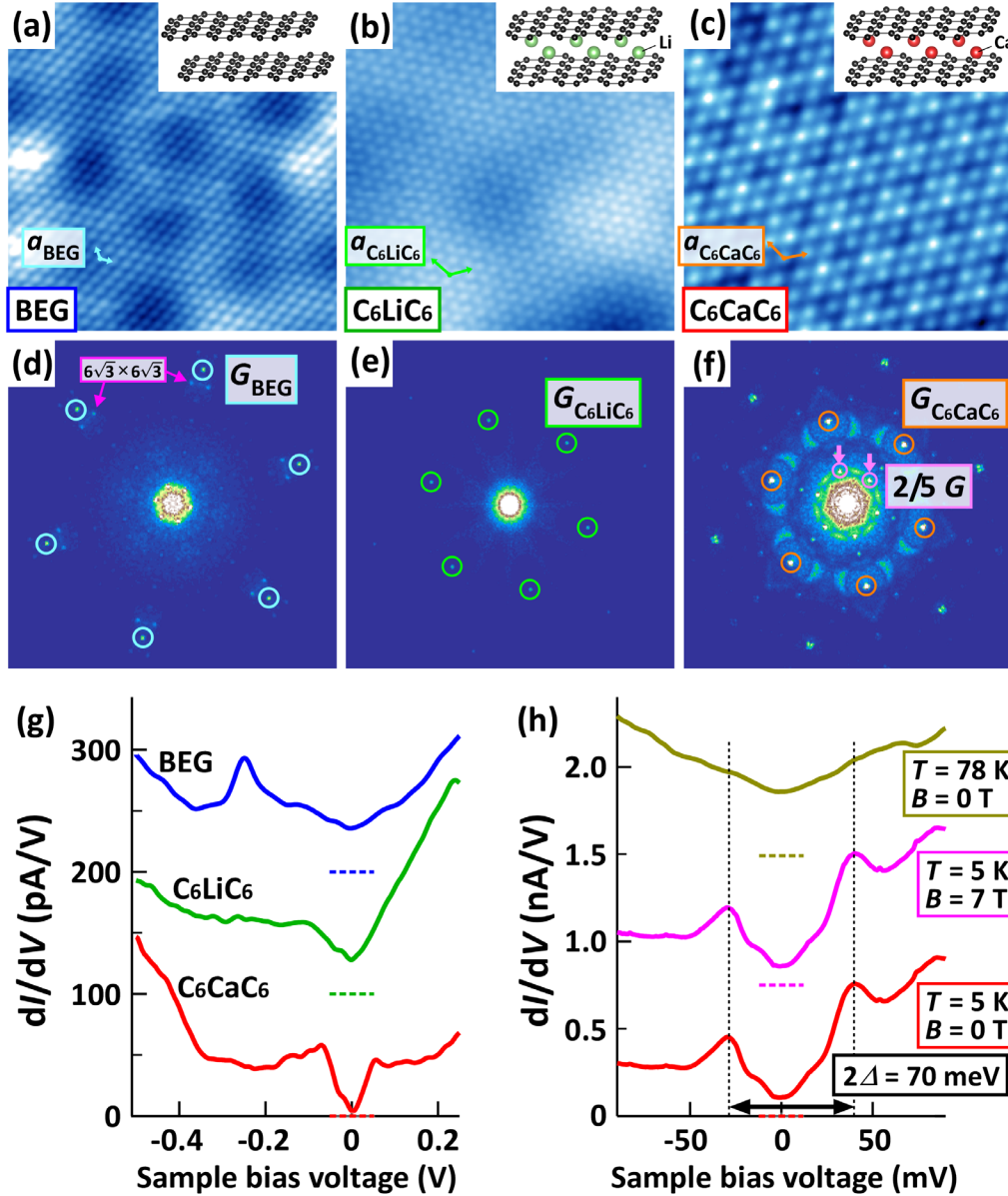


FIG. 1 (color online). Comparison of STM results for BEG, C_6LiC_6 , and C_6CaC_6 . (a)–(c) STM images of (a) BEG, obtained with a sample bias voltage (V_s) of -500 mV and a tunneling current (I_t) of 30 pA, (b) C_6LiC_6 ($V_s = -100$ mV, $I_t = 30$ pA), and (c) C_6CaC_6 ($V_s = -100$ mV, $I_t = 30$ pA). All the images were taken at 5 K in 6×6 nm². The arrows indicate the unit vectors. The insets show the schematic illustrations of each material. (d)–(f) FFT images of the corresponding STM images (a)–(c). Each FFT image is characterized by (d) the reciprocal lattice spot of G_{BEG} with the $(6\sqrt{3} \times 6\sqrt{3}) - R30^\circ$ satellite, (e) the additional spot ($G_{C_6LiC_6}$) with $(\sqrt{3} \times \sqrt{3}) - R30^\circ$ periodicity, and (f) the $(\sqrt{3} \times \sqrt{3}) - R30^\circ$ spot ($G_{C_6CaC_6}$) with a distinct spot corresponding to $2/5G_{C_6CaC_6}$. (g) Tunneling spectra obtained at 5 K for BEG, C_6LiC_6 , and C_6CaC_6 . The dashed lines show the zero differential conductance (dI/dV) level for each spectrum. For BEG and C_6LiC_6 , a broad gaplike feature is observed, while a clear gap structure is observed at the Fermi level for C_6CaC_6 . (h) Temperature (T) and magnetic-field (B) dependence of the tunneling spectra near the Fermi level in C_6CaC_6 . Each spectrum was obtained at 5 K in 0 T (red), at 5 K in 7 T (pink), and at 78 K in 0 T (olive), respectively. The gap structure is confirmed only at 5 K and is not affected by the external magnetic field. The value of the energy gap (2Δ) is evaluated to be around 70 meV.

on replacing Li with Ca, the STM image drastically changes into a new pattern, which is entirely different from those of BEG and C_6LiC_6 . Each Ca-intercalated site with $(\sqrt{3} \times \sqrt{3}) - R30^\circ$ periodicity, which corresponds to the $G_{C_6CaC_6}$ vector in the k space, becomes more prominent, suggesting a sizable contribution from the Ca atomic orbitals to the electronic states around the Fermi level [7,8]. Besides, a long-range modulation with a periodicity 2.5 times larger than that of C_6CaC_6 ($a_{C_6CaC_6}$) is clearly seen in Fig. 1(c) and is also confirmed by the sharp spot ($q^* = 2/5 G_{C_6CaC_6}$) in the FFT image [Fig. 1(f)]. This nonintegral spatial modulation cannot be explained in terms of surface reconstruction.

To address the above question, we measured the STS spectrum. As shown in Fig. 1(g), a clear energy gap with $2\Delta \sim 70$ meV is observed at 5 K under no magnetic field, while a broad gaplike structure is seen in both BEG and C_6LiC_6 [Fig. 1(g)]. Figure 1(h) shows the temperature and magnetic-field dependence of the STS spectrum for C_6CaC_6 , which indicates that the magnetic field does not affect the

spectrum. This result suggests that the gap structure does not have its origin in superconductivity, contrary to the theoretical predictions [5,6]. Here, it must be noted that the tunneling spectrum at 78 K does not show an apparent gap structure at the Fermi level, indicating that a phase transition, probably a CDW transition, may occur between 5 and 78 K.

Assuming that the CDW state emerges at low temperatures, it is important to determine the nesting condition required to drive the transition. In order to probe the behavior of electron scattering [17,18], the mapping of the local density of states (LDOS) near the Fermi level was performed at 5 K. Figure 2 shows the STS results for C_6CaC_6 : (a) topography, (b) conductance map at the Fermi level, and (c) its FFT image. In the conductance map, complex standing-wave patterns formed by electron scattering are confirmed in addition to the $2.5a_{C_6CaC_6}$ modulation. In the FFT image [Fig. 2(c)], several spots corresponding to the scattering vectors ($q_i; i = 1-6$) are also observed in addition to $G_{C_6CaC_6}$ and q^* .

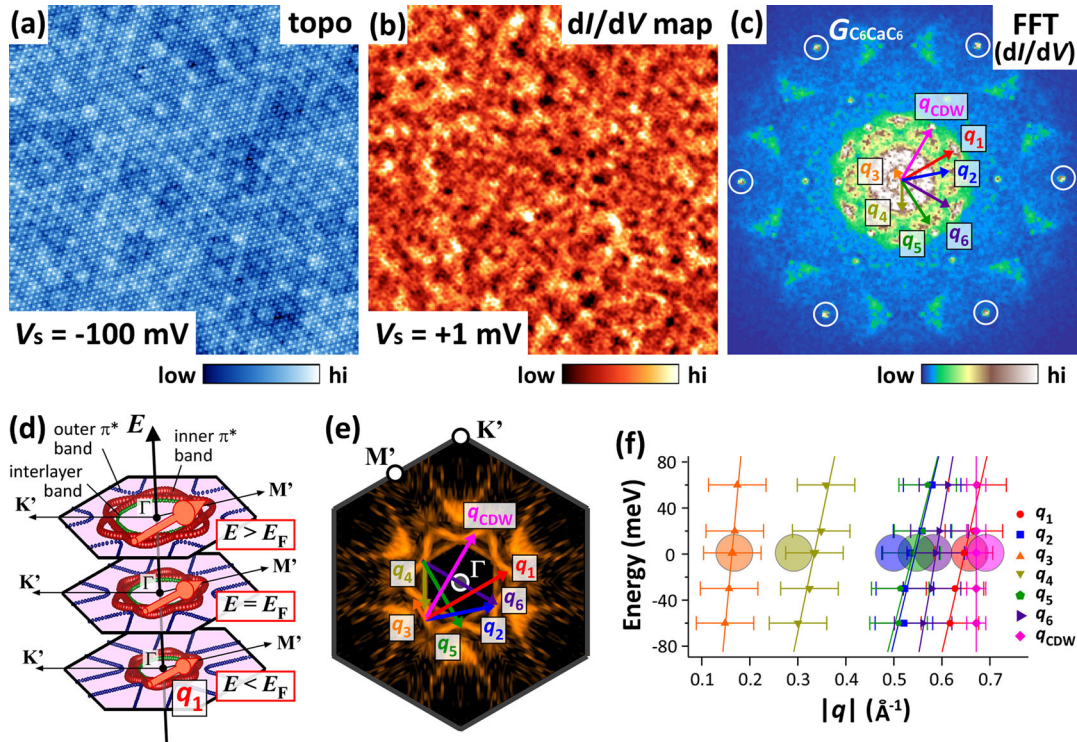


FIG. 2 (color online). STS results for C_6CaC_6 at 5 K under no magnetic field. (a) STM topographic image ($V_s = -100$ mV, $I_t = 30$ pA, 30×30 nm 2) obtained simultaneously with the STS measurement. (b) Differential conductance (dI/dV) map at $V_s = +1$ mV. Complex standing-wave patterns are observed with the $2.5a_{C_6CaC_6}$ topographic modulation. (c) FFT image of the dI/dV map at $V_s = +1$ mV. Several spots corresponding to scattering vectors are confirmed, as indicated by the q_i vectors in the FFT images. Note that the FFT image has been rotated for easy comparison with the image of the Fermi surface in Fig. 2(e). (d) A schematic illustration of the relationship between the electronic band structure and the scattering vector as a function of energy. The dotted lines denote the inner π^* band (red), the outer π^* band (blue), and the interlayer band (green). (e) Fermi surface of C_6CaC_6 obtained by the ARPES measurement, overlapped with the scattering vectors (q) observed in Fig. 2(c). All the q vectors fit in the large DOS sites of the inner π^* band. (f) The energy dependence of q vectors, obtained by energy-resolved LDOS mapping. Linear fitting lines have been appended in the chart as a guide for the eye. The large circles at the Fermi level show the magnitude of the scattering vectors ($|q|$), evaluated from the ARPES measurement.

It has been reported that the electronic structure near the Fermi level of C_6CaC_6 is composed of three different bands: an outer π^* band with a holelike dispersion, an inner π^* band with an electronlike dispersion, and an interlayer band with a free-electron-like dispersion [5–7]. As seen in Figs. 2(d) and 2(e), a good quantitative correspondence is seen between the q_i vectors and the large DOS sites of the inner π^* band observed in the ARPES measurement. It is noted that no other q_i vectors could be clearly found over the Brillouin zone in the FFT image [Fig. 2(c)], and we speculate that the q_i vectors are band-selectively detected in STM/STS. The magnitude of the q_i vectors systematically increases as the energy increases, reflecting the electronlike dispersion of the inner π^* band [Fig. 2(f)]. It is also clear in Fig. 2(e) that the q^* vector, which is responsible for the $2.5a_{C_6CaC_6}$ superstructure, bridges two sites of the inner π^* band on the Fermi surface. Thus, it is concluded that the CDW state emerges in C_6CaC_6 owing to the Fermi surface nesting of the π^* bands with the nesting vector $q_{CDW} = q^*$.

The Fermi surfaces of C_6LiC_6 and C_6CaC_6 are characterized by the snowflakelike hexagonal electron pockets (inner π^* band) around the Γ point and the triangular hole pocket (outer π^* band) centered at the K' point [7, 14]. Since the nesting condition is closely related to the character of Fermi surface [19], we expect that the CDW transition may also occur in both C_6LiC_6 and C_6CaC_6 . However, C_6LiC_6 shows no CDW transition, because neither a superstructure nor a clear gap is observed in C_6LiC_6 (Fig. 1). Therefore, it is inferred that the CDW transition may be strongly dependent on the magnitude of the Fermi-level shift, which reflects the carrier concentration ($\sim 2e^-$ per C_6CaC_6 unit cell [7] versus $\sim 1e^-$ per C_6LiC_6 unit cell [14]).

Here, we focus on the relationship between the CDW periodicity ($a_{CDW} = 5/2 a_{C_6CaC_6}$) and the epitaxial lattice of C_6CaC_6 on SiC. The ratio of the in-plane lattice constants in bulk is $|a_{C_6Ca}|/|a_{SiC}| = (0.4333 \text{ nm})/(0.3073 \text{ nm}) = 1.410$ [20], close to $7/5$. Therefore, it is reasonable that a commensurate lattice of the (5×5) C_6CaC_6 units per (7×7) SiC spacing ($a_{SiC} = 5/7 a_{C_6CaC_6}$) is formed [Fig. 3(a)]. In the k space, the commensuration corresponds to $G_{SiC} = 7/5 G_{C_6CaC_6}$, equivalent to $2/5 G_{C_6CaC_6}$, which perfectly matches the observed q^* vector [Fig. 3(b)]. On the other hand, the CDW transition is suppressed in C_6LiC_6 , in spite of the identical epitaxial relationship, because electron scattering ($q^* = 2/5 G_{C_6LiC_6}$) is not allowed, owing to the small Fermi surface [Fig. 3(b)]. Based on the above discussion, we conclude that the long-range potential modulation due to the SiC substrate triggers the CDW transition in C_6CaC_6 .

It has also been reported that single-crystalline bulk C_6Ca exhibits the CDW transition [13]. However, its origin is entirely different. The CDW state in bulk C_6Ca is characterized by a one-dimensional stripe pattern with (3×1) periodicity, while C_6CaC_6 shows the hexagonal and commensurate CDW periodicity of $(5/2 \times 5/2)$ coupled with the substrate lattices. In addition, the energy-gap value in bulk C_6Ca ($2\Delta \sim 450 \text{ meV}$) is 6–7 times larger than that of C_6CaC_6 ($2\Delta \sim 70 \text{ meV}$), and the transition temperature of around 240 K in the bulk crystal is much higher than that in the thin film, 77 K. Thus, the CDW state in C_6CaC_6 is a unique phenomenon induced by the substrate effect and intrinsically different from that in bulk.

Although theoretical studies have predicted the possibility of superconductivity in C_6CaC_6 [5, 6], no superconducting

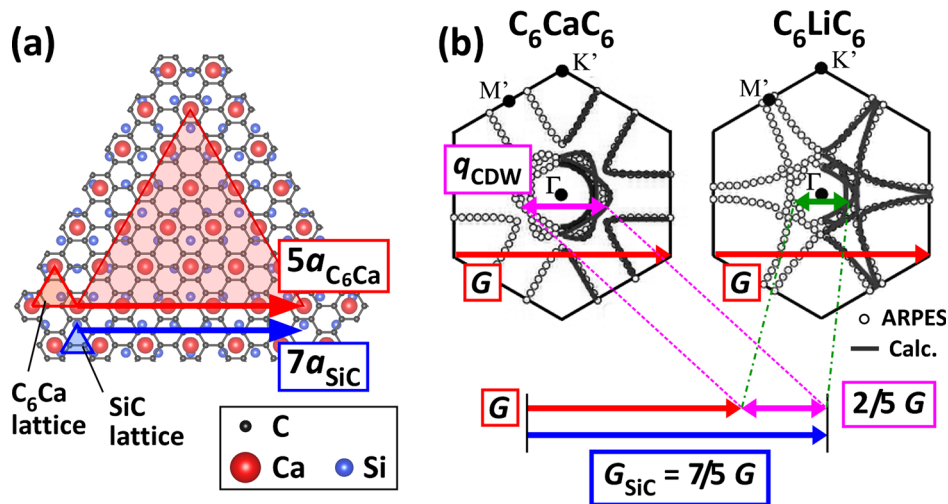


FIG. 3 (color online). The relationship between the commensurate lattice and the Fermi surface nesting of the CDW state in C_6CaC_6 on the SiC substrate. (a) The commensurate lattice of C_6CaC_6 on SiC in the r space. The (5×5) units of C_6CaC_6 cover the area of SiC (7×7) lattices ($a_{C_6CaC_6} : a_{SiC} = 7 : 5$). (b) Fermi surfaces of C_6CaC_6 and C_6LiC_6 and the nesting condition of the CDW state in C_6CaC_6 . The commensurate relationship in the k space between C_6CaC_6 and SiC perfectly matches the CDW nesting vector ($q_{CDW} = 2/5 G$). A comparison of the Fermi surface between C_6CaC_6 and C_6LiC_6 indicates that electron scattering with a scattering vector of $2/5 G$ is allowed in C_6CaC_6 , while it is forbidden in C_6LiC_6 because of the smaller Fermi surface.

transition has been observed in epitaxially grown C_6CaC_6 on SiC. The superconductivity in bulk GICs has been attributed to the interlayer band with a free-electron-like character around the Γ point [8]. In contrast, in bulk C_6Ca , a superconducting gap was observed in the π^* band as well as in the interlayer band [10], suggesting the contribution from the π^* band to the superconductivity. In Ca-intercalated bilayer graphene, on the other hand, we observe the gap feature in the π^* band induced by the CDW nesting. In this regard, it is speculated that the possible superconducting transition in C_6CaC_6 may be suppressed by the CDW nesting in the π^* band. This scenario supports a recent report on the superconductivity in Ca-intercalated thick multilayer graphene [21], in which the potential modulation at the interface should be significantly attenuated.

In conclusion, we have presented the results of low-temperature STM/STS and ARPES on epitaxially grown C_6CaC_6 to study the possibility of superconductivity in metal-intercalated bilayer graphene. We speculate that the superconductivity in C_6CaC_6 is suppressed by the SiC substrate. The charge-density wave (CDW) is induced by the potential modulation due to the commensurate lattice matching between the C_6CaC_6 film and the SiC substrate. This result suggests that the competition between superconductivity and CDW is prominent.

This work was partly supported by the Japanese Society for Promotion of Science (JSPS, KAKENHI: 23686002, 24740216, 26246022), the Japan Science and Technology Agency–Core Research for Evolutional Science and Technology (JST-CREST) program, and the Ministry of Education, Culture, Sports, Science, and Technology of Japan (MEXT, Grant-in-Aid for Scientific Research on Innovative Areas “Science of Atomic Layers” 25107003), and World Premier International Research Center, Advanced Institute for Materials Research.

[1] M. S. Dresselhaus and G. Dresselhaus, *Adv. Phys.* **51**, 1 (2002).

- [2] N. B. Hannay, T. H. Geballe, B. T. Matthias, K. Andres, P. Schmidt, and D. MacNair, *Phys. Rev. Lett.* **14**, 225 (1965).
- [3] T. E. Weller, M. Ellerby, S. S. Saxena, R. P. Smith, and N. T. Skipper, *Nat. Phys.* **1**, 39 (2005).
- [4] K. S. Novoselov, A. K. Geim, S. V. Morozov, D. Jiang, Y. Zhang, S. V. Dubonos, I. V. Grigorieva, and A. A. Firsov, *Science* **306**, 666 (2004).
- [5] I. I. Mazin and A. V. Balatsky, *Philos. Mag. Lett.* **90**, 731 (2010).
- [6] R. A. Jishi, D. M. Guzman, and H. M. Alyahyaei, *Adv. Studies Theor. Phys.* **5**, 703 (2011).
- [7] K. Kanetani, K. Sugawara, T. Sato, R. Shimizu, K. Iwaya, T. Hitosugi, and T. Takahashi, *Proc. Natl. Acad. Sci. USA* **109**, 19610 (2012).
- [8] G. Csányi, P. B. Littlewood, A. H. Nevidomskyy, C. J. Pickard, and B. D. Simons, *Nat. Phys.* **1**, 42 (2005).
- [9] K. Sugawara, T. Sato, and T. Takahashi, *Nat. Phys.* **5**, 40 (2009).
- [10] S.-L. Yang, J. A. Sobota, C. A. Howard, C. J. Pickard, M. Hashimoto, D. H. Lu, S.-K. Mo, P. S. Kirchmann, and Z.-X. Shen, *Nat. Commun.* **5**, 3493 (2014).
- [11] M.-H. Whangbo, W. Liang, J. Ren, S. N. Magonov, and A. Wawkuszewski, *J. Phys. Chem.* **98**, 7602 (1994).
- [12] A. L. Tchougréeff, *J. Phys. Chem.* **100**, 14048 (1996).
- [13] K. C. Rahnejat, C. A. Howard, N. E. Shuttlesworth, S. R. Schofield, K. Iwaya, C. F. Hirjibehedin, Ch. Renner, G. Aeppli, and M. Ellerby, *Nat. Commun.* **2**, 558 (2010).
- [14] K. Sugawara, K. Kanetani, T. Sato, and T. Takahashi, *AIP Adv.* **1**, 022103 (2011).
- [15] K. Iwaya, R. Shimizu, T. Hashizume, and T. Hitosugi, *Rev. Sci. Instrum.* **82**, 083702 (2011).
- [16] C. Riedl, C. Coletti, and U. Starke, *J. Phys. D* **43**, 374009 (2010).
- [17] M. F. Crommie, C. P. Lutz, and D. M. Eigler, *Nature (London)* **363**, 524 (1993).
- [18] L. Petersen, Ph. Hofmann, E. W. Plummer, and F. Besenbacher, *J. Electron Spectrosc. Relat. Phenom.* **109**, 97 (2000).
- [19] G. Grüner, *Density Waves in Solids* (Westview Press, Boulder, 1994).
- [20] N. Emery, C. Hérod, J.-F. Marêché, and P. Lagrange, *Sci. Tech. Adv. Mater.* **9**, 044102 (2008).
- [21] K. Li, X. Feng, W. Zhang, Y. Ou, L. Chen, K. He, L.-L. Wang, L. Guo, G. Liu, Q.-K. Xue, and X. Ma, *Appl. Phys. Lett.* **103**, 062601 (2013).